

# Super-resolution Imaging of Fluorescent Dipoles by Polarized Structured Illumination Microscopy

Karl Zhanghao<sup>1,\*†</sup>, Xingye Chen<sup>2,\*</sup>, Wenhui Liu<sup>2</sup>, Chuanyan Shan<sup>3</sup>, Kun Zhao<sup>1</sup>, Meiqi Li<sup>1</sup>, Amit Lai<sup>1</sup>, Qionghai Dai<sup>2,†</sup>, Peng Xi<sup>1,†</sup>

<sup>1</sup> Department of Biomedical Engineering, College of Engineering, Peking University, Beijing 100871, China

<sup>2</sup> Department of Automation, Tsinghua University, Beijing 100084, China

<sup>3</sup> Department of Life Sciences, Peking University, Beijing 100871, China

\* These authors contributed equally to this work.

† Correspondence: P.X. (xipeng@pku.edu.cn), Q.D. (daiqh@tsinghua.edu.cn), K.Z. (karl.hao.zhang@gmail.com)

Fluorescent dipoles reflect the spatial orientation of the fluorophores, which indicates structural information of the targeted proteins. As an important super-resolution technique, Structured Illumination Microscopy (SIM) requires three different couples of linearly polarized light to generate high-contrast interferometric fringes, relating to polarization modulation, a technique to measure dipole orientations[1, 2, 3]. Here we reveal the inherent connection between SIM and polarization modulation: exciting fluorescent anisotropic specimens using a linearly polarized light is a type of structured illumination in the dimension of dipole orientation, with polarization modulation varying the phases of the pattern. Further, we invented polarized SIM (pSIM) with super-resolution imaging of the fluorescent dipoles, through expanding the spatial and polarization observable region in reciprocal space. pSIM maintains all the advantages of SIM and can be performed directly on the existing commercial SIM microscopes. We believe pSIM would become a powerful and widely accessible technique in studying biological structures.

Fluorescence Polarization Microscopy (FPM) has been widely applied to study the molecular structure of fluorophores and targeted proteins, including the area of cell membranes[4, 5], biological filaments[1, 6] and macromolecules[7, 8, 9]. Due to the low pass filtering nature of optical imaging process, FPM suffers from the Abbe's diffraction limit, which deteriorates the imaging accuracy of both position and orientation of the fluorescent dipoles. Various super-resolution FPM techniques have therefore been developed to provide resolution beyond the diffraction barrier: (1) super resolution by polarization demodulation using linear dichroism imaging system[2, 3]; (2) Excitation Polarization Angle Narrowing (ExPAN) by STimulated Emission Depletion (STED)[3]; (3) single fluorescent dipole imaging by polarized STORM[10, 11] or single fluorescent dipole tracking[10, 12, 13, 14]. However, the polarization demodulation methods have limited resolution of 150 nm and the actual resolution varied with samples[2]. The ExPAN method only increases the accuracy of orientation detection without spatial resolution enhancement[3]. Single molecular methods either take tens of minutes imaging time or apply to sparsely labeled samples[12, 13, 14].

SIM has been demonstrated to be very compatible with live-cell imaging due to its fast imaging speed and low photo-toxicity. It extracts finer features of the specimen by applying sinusoidal illumination patterns with three orientations and three phases. Polarization control is required in most SIM systems to achieve high-contrast illumination patterns. Almost the same polarization modulation optics appear in the system of Linear Dichroism (LD) (Figure 1 a, b), which utilizes rotational modulation of the excitation polarization direction to measure the dipole orientations[1, 2, 3]. More interestingly, the similar pattern of SIM in spatial dimensions and polarization excitation in dipole orientation dimension reminds us to correlate this two distinct approaches (Figure 1 c, d). Based on the similarity between SIM and LD, we believe the potential of SIM to be a perfect super-resolution FPM. In this paper, we first prove that linear dichroism is intrinsically equivalent to structured illumination in orientation dimension. Afterwards, we demonstrated the principle of how pSIM achieves super-resolution imaging of fluorescent dipoles. Finally, we proposed approaches

to achieve finer dipole orientation imaging, either by combination of LD and polarization detection or by non-linear polarization excitation.

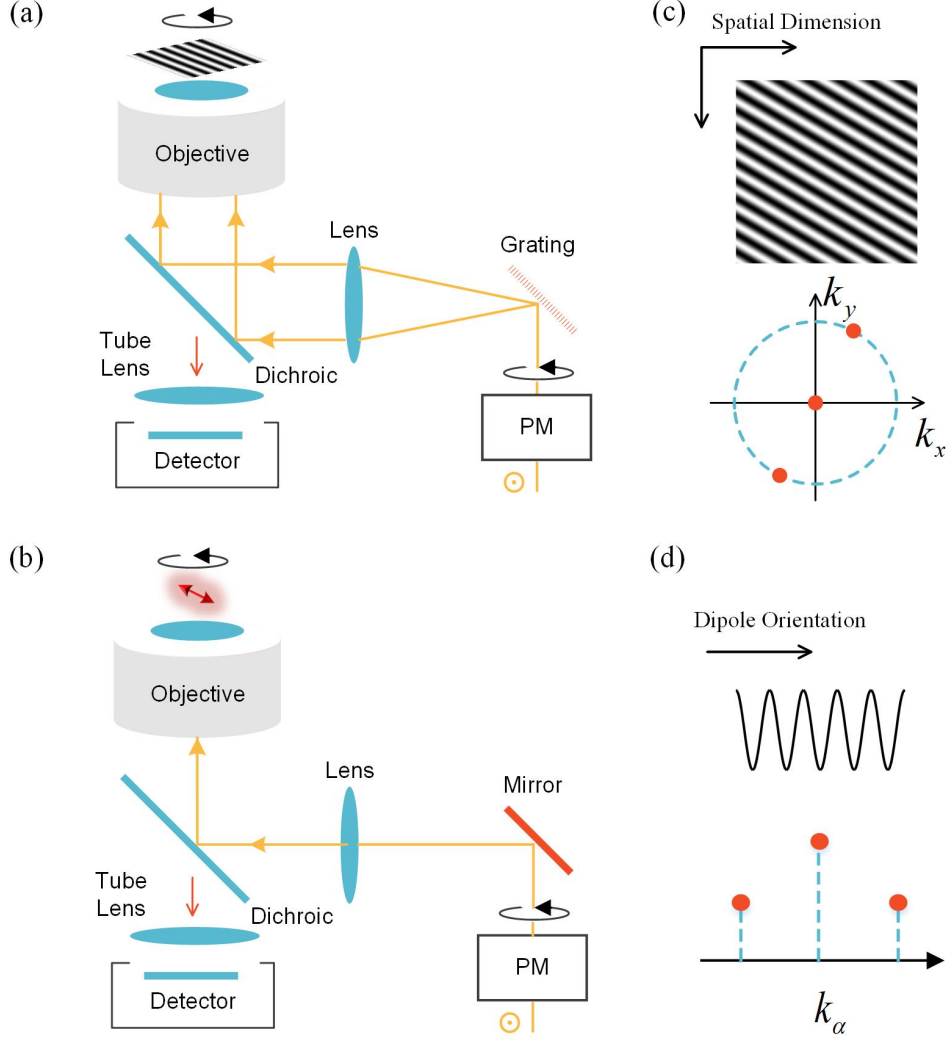


Figure 1: **Comparison between SIM and LD.** (a) SIM uses two s-polarized lasers for high-contrast interferometric fringes, which requires polarization modulation (PM) synchronized with the rotation of gratings. (b) LD uses three or more excitation polarization angles to measure the orientation of fluorescent dipoles. Except for the grating, LD uses almost identical hardware presented in SIM. (c) In SIM, when a spatial sinusoidal illumination is used to illuminate the specimen, the output signal is their product. (d) Exciting fluorescent anisotropic specimen using a linearly polarized laser achieves similar sinusoidal illumination on orientation dimension. The Fourier transform of a sinusoidal signal (spatial or orientational) contains only three components: a DC component and two conjugated peaks.

**Comparison between SIM and LD.** SIM uses a spatial sinusoidal pattern  $\tilde{I}_{\theta,\phi}(\mathbf{k}_r)$  to illuminate the specimen  $S(\mathbf{r})$ , which is assumed with isotropic fluorescence polarization. The polarization modulation in SIM is to maintain high-contrast interferometric fringes. In contrast, LD uses polarization excitation to

achieve sinusoidal illumination  $F_\theta(\alpha)$  in polarization dimension.

$$SIM : \quad D_{\theta,\phi}(\mathbf{r}) = \underbrace{[S(\mathbf{r}) \cdot I_{\theta,\phi}(\mathbf{r})]}_{Excitation} \otimes PSF(\mathbf{r}); I_{\theta,\phi}(\mathbf{r}) = \frac{I_0}{2} [1 + \cos(2\pi \mathbf{p}_\theta \cdot \mathbf{r} + \phi)] \quad (1)$$

$$LD : \quad D_{\theta,\phi}(\mathbf{r}; \alpha) = \underbrace{[S(\mathbf{r}) \cdot F_\theta(\alpha)]}_{Excitation} \otimes PSF(\mathbf{r}; \alpha); F_\theta(\alpha) = \frac{\eta}{2} [1 + \cos(2\pi \cdot \frac{1}{\pi} \cdot \alpha - 2\theta)] \quad (2)$$

Here,  $\mathbf{r}$  denotes spatial coordinate and  $\alpha$  denotes dipole orientation coordinate.  $\theta$  is the direction of interferometric fringes or the direction of polarization, which are required to be the same for high-contrast patterns.  $I_0$  is the laser power and  $\eta$  is the exaction efficiency.  $S(\mathbf{r})$  means polarization-isotropic specimen and  $S_p(\mathbf{r}, \alpha)$  means polarization-anisotropic specimen.  $PSF(\mathbf{r})$  is the point spread function (PSF) of the system. In (2), both system PSF and detected image are written as  $PSF(\mathbf{r}; \alpha)$  and  $D_\theta(\mathbf{r}; \alpha)$  for consistency of the expression. Indeed, the LD system could not distinguish polarized fluorescence. The fluorescent signals of every polarization are integrated by the detector, which means convolution with a constant function:  $PSF(\mathbf{r}; \alpha) = PSF(\mathbf{r}) \cdot \omega(\alpha)$ , where  $\omega(\alpha) = 1$  for  $0 \leq \alpha \leq \pi$ . Since the system Optical Transfer Function (OTF) is the Fourier transform of PSF, the spatial-orientational  $OTF(\mathbf{k}_r, k_\alpha)$  would be equal to  $OTF(\mathbf{k}_r) \cdot \delta(k_\alpha)$ , which only has zero frequency component in orientation dimension.

$$SIM : \quad \tilde{D}_{\theta,\phi}(\mathbf{k}_r) = [\tilde{S}(\mathbf{k}_r) \otimes \tilde{I}_{\theta,\phi}(\mathbf{k}_r)] \cdot OTF(\mathbf{k}_r); \quad (3)$$

$$I_{\theta,\phi}(\mathbf{k}_r) = \frac{\pi I_0}{4} [\delta(\mathbf{k}_r) + \frac{1}{2} e^{i\phi} \delta(\mathbf{k}_r - \mathbf{k}_\theta) + \frac{1}{2} e^{-i\phi} \delta(\mathbf{k}_r + \mathbf{k}_\theta)]$$

$$LD : \quad \tilde{D}_\theta(\mathbf{k}_r, k_\alpha) = [\tilde{S}_p(\mathbf{k}_r, k_\alpha) \otimes \tilde{F}_\theta(k_\alpha)] \cdot OTF(\mathbf{k}_r, k_\alpha); \quad (4)$$

$$\tilde{F}_\theta(k_\alpha) = \frac{\pi\eta}{4} [\delta(k_\alpha) + \frac{1}{2} e^{-i2\theta} \delta(k_\alpha - \frac{1}{\pi}) + \frac{1}{2} e^{i2\theta} \delta(k_\alpha + \frac{1}{\pi})]$$

(3) and (4) is achieved by applying Fourier transform to (1) and (2). Both  $\tilde{I}_{\theta,\phi}(\mathbf{k}_r)$  and  $\tilde{F}_\theta(\mathbf{k}_r, k_\alpha)$  have 3 frequency components (**Figure 1 e, f**). The convolution of  $\tilde{S}(\mathbf{k}_r) \otimes \tilde{I}_{\theta,\phi}(\mathbf{k}_r)$  or  $\tilde{S}_p(\mathbf{k}_r, k_\alpha) \otimes \tilde{F}_\theta(k_\alpha)$  brings 3 copies of the specimen information  $\tilde{S}$  or  $\tilde{S}_p$ , two of which have their higher frequency components moved into observable region in reciprocal space, bringing super-resolution. With 3 different directions of structured illumination, 7 spatial frequency components (except 2 redundant components) are acquired by SIM:  $\tilde{S}(\mathbf{k}_r)$ ,  $\tilde{S}(\mathbf{k}_r - \mathbf{k}_{\theta_1})$ ,  $\tilde{S}(\mathbf{k}_r + \mathbf{k}_{\theta_1})$ ,  $\tilde{S}(\mathbf{k}_r - \mathbf{k}_{\theta_2})$ ,  $\tilde{S}(\mathbf{k}_r + \mathbf{k}_{\theta_2})$ ,  $\tilde{S}(\mathbf{k}_r - \mathbf{k}_{\theta_3})$ ,  $\tilde{S}(\mathbf{k}_r + \mathbf{k}_{\theta_3})$ , doubling the spatial resolution (**Figure 2 b**). With 3 or more polarization directions, 3 orientational frequency components are acquired by LD:  $\tilde{S}_p(\mathbf{k}_r, k_\alpha)$ ,  $\tilde{S}_p(\mathbf{k}_r, k_\alpha - \frac{1}{\pi})$ ,  $\tilde{S}_p(\mathbf{k}_r, k_\alpha + \frac{1}{\pi})$ , enabling dipole orientation imaging (**Figure 2 c**).

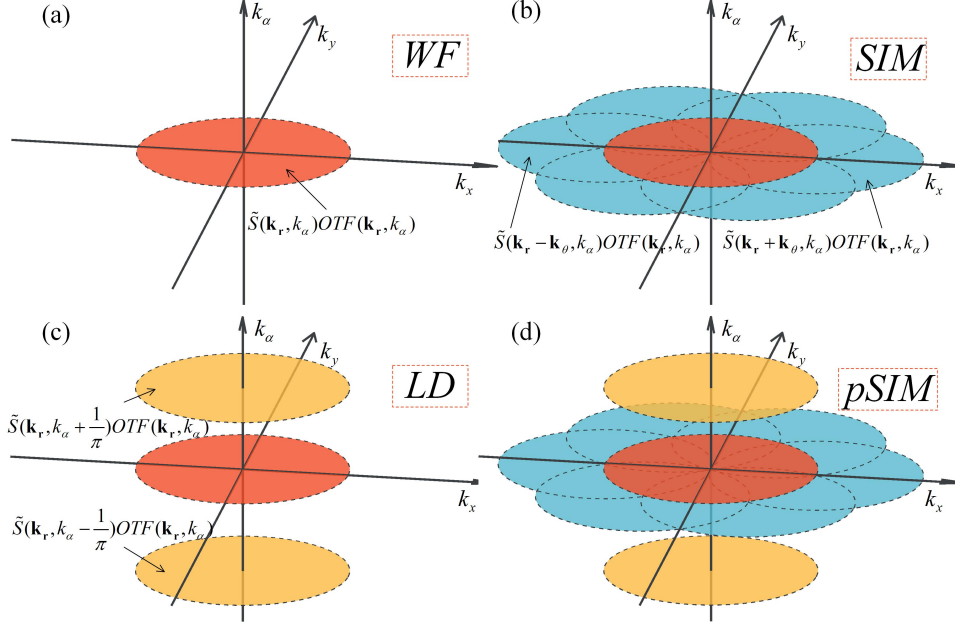


Figure 2: **Comparison of the observable region of reciprocal space among wide field (a), SIM (b), LD (c), and pSIM (d).** (a) Due to the optical transfer function (OTF) cut-off of a wide-field microscope, the frequency outside the passband is blocked. (b) In frequency domain, the product of specimen and modulation frequency becomes convolution, which expands the visible frequency with 6 pedals. (c) The polarization modulation also brings two additional orientational components in the reciprocal space. (d) Combining SIM with polarization modulation leads to super-resolution polarization microscopy, which expands both the spatial and orientational observable region.

**Principle of pSIM.** SIM assumes the isotropic fluorescence polarization of specimen, which is not valid in many samples, such as membrane structures and filamentous structures. With remodeling the sample considering fluorescence polarization would extend the application of SIM on any kind of samples, as well as enabling measurement of dipole orientations. For pSIM, when the sample is illuminated under the polarized structured illumination, the detected images and their Fourier transform would be:

$$D_{\theta,\phi}(\mathbf{r}, \alpha) = [S_p(\mathbf{r}, \alpha) \cdot I_{\theta,\phi}(\mathbf{r}) \cdot F_\theta(\alpha)] \otimes PSF(\mathbf{r}, \alpha) \quad (5)$$

$$\tilde{D}_{\theta,\phi}(\mathbf{k}_r, k_\alpha) = [\tilde{S}_p(\mathbf{k}_r, k_\alpha) \otimes \tilde{I}_{\theta,\phi}(\mathbf{k}_r) \otimes \tilde{F}_\theta(\alpha)] \cdot OTF(\mathbf{k}_r, k_\alpha) \quad (6)$$

Both the spatial structured illumination  $I_{\theta,\phi}(\mathbf{r})$  and orientational structured illumination  $F_\theta(\alpha)$  bring larger observable reciprocal space, on spatial dimensions and polarization dimensions. The reconstruction of pSIM takes two steps: "SIM step" and "LD step". For "SIM step", the 9 frequency components are solved just the same as SIM (Eq. 7), but with convolution with polarization terms  $\tilde{F}_\theta(k_\alpha)$ . There are 3 frequency components solved in each pattern direction and 3 pattern directions.

$$\begin{bmatrix} \tilde{D}_{\theta_i, \phi_1}(\mathbf{k}_r, k_\alpha) \\ \tilde{D}_{\theta_i, \phi_2}(\mathbf{k}_r, k_\alpha) \\ \tilde{D}_{\theta_i, \phi_3}(\mathbf{k}_r, k_\alpha) \end{bmatrix} = M_{SIM} \cdot \begin{bmatrix} [\tilde{S}_p(\mathbf{k}_r, k_\alpha) \otimes \tilde{F}_{\theta_i}(k_\alpha)] \cdot OTF(\mathbf{k}_r, k_\alpha) \\ [\tilde{S}_p(\mathbf{k}_r - \mathbf{k}_{\theta_i}, k_\alpha) \otimes \tilde{F}_{\theta_i}(k_\alpha)] \cdot OTF(\mathbf{k}_r, k_\alpha) \\ [\tilde{S}_p(\mathbf{k}_r + \mathbf{k}_{\theta_i}, k_\alpha) \otimes \tilde{F}_{\theta_i}(k_\alpha)] \cdot OTF(\mathbf{k}_r, k_\alpha) \end{bmatrix}; M_{SIM} = \frac{\pi I_0}{4} \begin{bmatrix} 1 & \frac{1}{2}e^{i\phi_1} & \frac{1}{2}e^{+i\phi_1} \\ 1 & \frac{1}{2}e^{i\phi_2} & \frac{1}{2}e^{+i\phi_2} \\ 1 & \frac{1}{2}e^{i\phi_3} & \frac{1}{2}e^{+i\phi_3} \end{bmatrix} \quad (7)$$

$$\begin{bmatrix} \tilde{S}_p(\mathbf{k}_r, k_\alpha) \otimes \tilde{F}_{\theta_1}(k_\alpha) \\ \tilde{S}_p(\mathbf{k}_r, k_\alpha) \otimes \tilde{F}_{\theta_2}(k_\alpha) \\ \tilde{S}_p(\mathbf{k}_r, k_\alpha) \otimes \tilde{F}_{\theta_3}(k_\alpha) \end{bmatrix} = M_{LD} \cdot \begin{bmatrix} \tilde{S}_p(\mathbf{k}_r, k_\alpha) \cdot OTF(\mathbf{k}_r, k_\alpha) \\ \tilde{S}_p(\mathbf{k}_r, k_\alpha - \frac{1}{\pi}) \cdot OTF(\mathbf{k}_r, k_\alpha) \\ \tilde{S}_p(\mathbf{k}_r, k_\alpha + \frac{1}{\pi}) \cdot OTF(\mathbf{k}_r, k_\alpha) \end{bmatrix}; M_{LD} = \frac{\pi\eta}{4} \begin{bmatrix} 1 & \frac{1}{2}e^{-i2\theta_1} & \frac{1}{2}e^{+i2\theta_1} \\ 1 & \frac{1}{2}e^{-i2\theta_2} & \frac{1}{2}e^{+i2\theta_2} \\ 1 & \frac{1}{2}e^{-i2\theta_3} & \frac{1}{2}e^{+i2\theta_3} \end{bmatrix} \quad (8)$$

Then "LD step" follows. From the 3 original spatial components  $\tilde{S}_p(\mathbf{k}_r, k_\alpha) \otimes \tilde{F}_{\theta_i}(k_\alpha)$ ,  $i = 1, 2, 3$ ,  $\tilde{S}_p(\mathbf{k}_r, k_\alpha)$ ,  $\tilde{S}_p(\mathbf{k}_r, k_\alpha - \frac{1}{\pi})$ ,  $\tilde{S}_p(\mathbf{k}_r, k_\alpha + \frac{1}{\pi})$  could be further solved the same as LD (Eq. 8). Its lucky for SIM to use 3 directions of illumination patterns, which cover the doubled region in reciprocal space. The 3 directions of polarization is just sufficient to extract the dipole orientations, while LD systems usually use more excitation polarizations to obtain robust results.

These 3 components solved in "LD step", together with other 6 components ( $\tilde{S}_p(\mathbf{k}_r \pm \mathbf{k}_{\theta_i}, k_\alpha) \otimes \tilde{F}_{\theta_i}(k_\alpha)$ ,  $i = 1, 2, 3$ ) solved in "SIM step" make up the observable region of reciprocal space of pSIM (**Figure 2 d**). The 6 high-order spatial components ( $\tilde{S}_p(\mathbf{k}_r \pm \mathbf{k}_{\theta_i}, k_\alpha) \otimes \tilde{F}_{\theta_i}(k_\alpha)$ ,  $i = 1, 2, 3$ ) couldnt be solved further to get separated polarization components  $\tilde{S}_p(\mathbf{k}_r \pm \mathbf{k}_{\theta_i}, k_\alpha)$  and  $\tilde{S}_p(\mathbf{k}_r \pm \mathbf{k}_{\theta_i}, k_\alpha) \pm \frac{1}{\pi}$ ,  $i = 1, 2, 3$  (**Supplementary Note 1**). Assembling the 9 shifted components in reciprocal space and applying inverse Fourier transform, spatial-orientational information of the specimen could be achieved in super-resolution. Conveniently, the dipole orientations are equivalent to the phases of the one-time-frequency component  $\tilde{S}_p(\mathbf{k}_r, k_\alpha - \frac{1}{\pi})$ .

To verify pSIM technique, we imaged actin filaments in BAPE cells labeled with Alexa 488 phalloidin, which has been demonstrated with strong fluorescence anisotropy (**Supplementary Movie 2**). From the 9 raw SIM images, we could observe both structured illumination and fluorescence intensity changes of individual actin filaments under different illumination patterns, due to the change of excitation polarization (**Supplementary Movie 1**). After solving the 9 frequency components using (7) and (8), wide field result, SIM result, LD result and pSIM result (**Figure 3**) could be obtained from the corresponding observable region in **Figure 2**. LD result has the same spatial resolution with WF results, while SIM/pSIM has doubled spatial resolution. With two orientational one-time-frequency components, LD and pSIM could measure the dipole orientations of the fluorophores. The dipole orientations of Alexa 488 phalloidin are mostly perpendicular to the direction of filaments, which is consistent with our previous results[2].

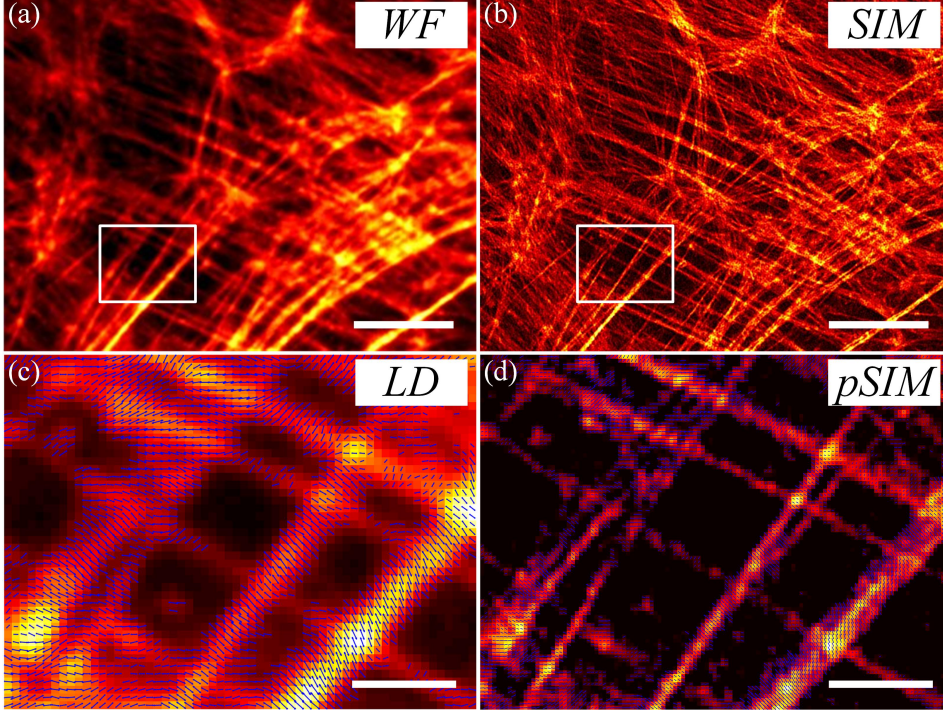


Figure 3: **Imaging results of Alexa 488 labeled actin filaments.** (a) Wide field results using frequency component ; (b) SIM results using 7 frequency components of  $\tilde{S}(\mathbf{k}_r)$ ,  $\tilde{S}(\mathbf{k}_r \pm \mathbf{k}_{\theta_i})$ ,  $i = 1, 2, 3$ ; (c) linear dichroism results using 3 frequency components:  $\tilde{S}_p(\mathbf{k}_r, k_\alpha)$ ,  $\tilde{S}_p(\mathbf{k}_r, k_\alpha - \frac{1}{\pi})$  and  $\tilde{S}_p(\mathbf{k}_r, k_\alpha + \frac{1}{\pi})$ ; (d) polarized SIM results using all the 9 frequency components. (c, d) are zoomed-images of the rectangle marked in (a, b). The dipole orientations are mapped with blue arrows with their directions. SIM and pSIM results have identical spatial resolution. Scale bar: (a, b)  $\mu m$ , (c, d)  $1 \mu m$ .

**Super-resolution in Orientation Imaging.** So far, the orientational resolution of pSIM is still limited by the FWHM of the  $\cos^2(\alpha - \theta)$  function, which would be further improved as exemplified below. Fluorescence Anisotropy (FA) is another type of FPM, which measures the emitted fluorescence polarization, by using a polarizer with various directions or polarization beam splitter[7, 14, 15]. Since the emitted fluorescence of the dipoles has the same cosine-square relation between orientation and polarization, the system OTF itself of FA ( $OTF_{FA}$ ) contains orientational one-time-frequency components. Thus, both FA and LD detect orientational one-time-frequency components, which obtains a sinusoidal intensity distribution of dipole orientations. In this case, the specimen could be modeled with one average dipole in each pixel[2], which could be indicated by an arrow imposed on the image, as shown in **Figure 3**. The different physical process behind LD and FA make it possible to combine them to achieve super-resolution dipole orientation imaging with second-order frequency components detected (**Figure S1**). Two Photon Excitation (TPE) usually has the nonlinear polarization excitation  $F_\theta(\alpha) = \cos^4(\alpha - \theta)$ [5] and could also detect second-order frequency components. By stimulated emission depletion, the nonlinear polarization excitation of ExPAN has even more higher-order frequency components, which further expands orientational observable region like nonlinear SIM. When second-order frequency components or higher-order components are detected, dipoles of different orientations in the same position may be distinguished. In this case, a full description of the specimen should be in the spatial-orientational  $(x, y, \alpha)$  coordinate (**Figure S2**).

In this work, we revealed the similarity between structured illumination and polarization excitation. Since the commercial SIM setup employs both hardware, super-resolution spatial and orientational imaging

could be achieved by pSIM, whose orientational resolution could be further improved with higher-order frequency components obtained. Though not demonstrated, 3D-pSIM could be performed on 3D-SIM system with similar principle. However, only 2D dipole orientation can be imaged, since 3D-SIM only has in-plane excitation polarization. pSIM principle is also compatible with high-NA TIRF-SIM[16] with higher resolution. With 100-nm lateral resolution, 300-nm axial resolution, as fast as 100 f.p.s. imaging speed[17], and orientation imaging of fluorescent dipoles, pSIM should become one of the most powerful super-resolution FPM technique, accompanied with its compatibility with existing commercial equipment. We believe pSIM to be a widely applied tool in studying the molecular dynamics of biological structures.

**Methods** Alexa 488 Phalloidin labeled actin sample is purchased from ThermoFisher (Fluocells Prepared Slide #1, F36924). SIM imaging was performed on a commercial system (DeltaVision OMX SR, GE, US), with 60X 1.4 N.A. oil immersion objective (Olympus, Japan) and AF488 filter sets. Standard 2D SIM sequence was performed with image pixel size of 80 nm. OMX system exported illumination parameters and raw images, which were then analyzed by the algorithm in the article.

**Author Contributions** KZ conceived the project. PX and QD supervised the research. KZ, XC, WL and CS completed the theory and experiments. PX, KZ, and XC wrote the manuscript with inputs from all authors.

**Acknowledgments** This work was supported by the National Key Research and Development Program of China (2017YFC0110202), the National Instrument Development Special Program (2013YQ03065102), the National Natural Science Foundation of China (61475010, 61729501, 61327902), and the Science and Technology Commission of the Shanghai Municipality (16DZ1100300). We thank the Core Facilities of Life Sciences, Peking University for assistance with SIM Imaging.

## A. SUPPLEMENTARY NOTE 1: DERIVATION OF PSIM

In FPM system, the fluorescence anisotropic sample  $S_p(\mathbf{r}, \alpha)$  is modulated by the excitation efficiency function  $F(\mathbf{r}, \alpha)$ , and blurred with a point spread function  $PSF(\mathbf{r}, \alpha)$ , where  $\alpha$  denotes the orientation and  $\mathbf{r}$  denotes the spatial position. The signal on the image plane  $D(\mathbf{r}, \alpha)$  can be represented as:

$$D(\mathbf{r}, \alpha) = [S_p(\mathbf{r}, \alpha) \cdot F(\mathbf{r}, \alpha)] \otimes PSF(\mathbf{r}, \alpha) \quad (S1)$$

Since the common-used sensor (CCD, sCMOS) is not sensitive to the polarization angle, so the detected image  $I(\mathbf{r})$  is the integration of the signal in every polarization:

$$I(\mathbf{r}) = \int_{\alpha} D(\mathbf{r}, \alpha) d\alpha \quad (S2)$$

The corresponding form of (S2) in Fourier domain is:

$$\tilde{I}(\mathbf{k}_r) = \tilde{D}(\mathbf{k}_r, k_{\alpha})|_{k_{\alpha}=0} = \tilde{D}(\mathbf{k}_r, 0) \quad (S3)$$

It means that the detected image only zero-frequency component in orientation dimension. In other word, the  $PSF(\mathbf{r}, \alpha)$ , and  $OTF(\mathbf{k}_r, k_{\alpha})$  of the system can be represented as:

$$\begin{aligned} PSF(\mathbf{r}, \alpha) &= PSF(\mathbf{r}) \cdot \omega(\alpha), \text{ where } \omega(\alpha) = 1, \text{ for } 0 \leq \alpha \leq \pi \\ OTF(\mathbf{k}_r, k_{\alpha}) &= OTF(\mathbf{k}_r) \cdot \delta(\alpha) \end{aligned} \quad (S4)$$

For pSIM, the specimen is illuminated with a spatial sinusoidal pattern  $I_{\theta, \phi}(\mathbf{r}) = \frac{I_0}{2} [1 + \cos(2\pi \mathbf{p}_{\theta} \cdot \mathbf{r}) + \phi]$ . Since in a typical SIM systems, the polarization of the illumination light is the same as  $\theta$ , so the signal on the image plane  $D_{\theta, \phi}(\mathbf{r}, \alpha)$  can be represented as[2, 3]:

$$\begin{aligned} D_{\theta, \phi} &= [S_p(\mathbf{r}, \alpha) \cdot I_{\theta, \phi}(\mathbf{r}) \cdot F_{\theta}(\alpha)] \otimes PSF(\mathbf{r}, \alpha), \\ \text{where } I_{\theta, \phi}(\mathbf{r}) &= \frac{I_0}{2} [1 + \cos(2\pi \mathbf{p}_{\theta} \cdot \mathbf{r}) + \phi], \\ F_{\theta}(\alpha) &= \cos^2(\theta - \alpha). \end{aligned} \quad (S5)$$

The Fourier transform of (S5) is:

$$\begin{aligned} \tilde{D}_{\theta, \phi}(\mathbf{k}_r, k_{\alpha}) &= [\tilde{S}_p(\mathbf{k}_r, k_{\alpha}) \otimes \tilde{I}_{\theta, \phi}(\mathbf{k}_r \otimes \tilde{F}_{\theta}(\alpha))] \cdot OTF(\mathbf{k}_r, k_{\alpha}) \\ &= \frac{\eta I_0}{2} \left\{ \begin{aligned} &\tilde{S}_p(\mathbf{k}_r, k_{\alpha}) \otimes [\delta(\mathbf{k}_r) + \frac{1}{2}\delta(\mathbf{k}_r - \mathbf{k}_{\theta})e^{i\phi} + \frac{1}{2}\delta(\mathbf{k}_r + \mathbf{k}_{\theta})e^{-i\phi}] \\ &\otimes [\delta(k_{\alpha}) + \frac{1}{2}\delta(k_{\alpha} - \frac{1}{\pi})e^{-i2\theta} + \frac{1}{2}\delta(k_{\alpha} + \frac{1}{\pi})e^{i2\theta}] \end{aligned} \right\} \cdot OTF(\mathbf{k}_r, k_{\alpha}) \\ &= \frac{\eta I_0}{2} \left\{ \begin{aligned} &\tilde{S}_p(\mathbf{k}_r, k_{\alpha}) + \frac{1}{2}\tilde{S}_p(\mathbf{k}_r, k_{\alpha} - \frac{1}{\pi})e^{-i2\theta} + \frac{1}{2}\tilde{S}_p(\mathbf{k}_r, k_{\alpha} + \frac{1}{\pi})e^{i2\theta} \\ &+ e^{i\phi}[\tilde{S}_p(\mathbf{k}_r - \mathbf{k}_{\theta}, k_{\alpha}) + \frac{1}{2}\tilde{S}_p(\mathbf{k}_r - \mathbf{k}_{\theta}, k_{\alpha} - \frac{1}{\pi})e^{-i2\theta} + \frac{1}{2}\tilde{S}_p(\mathbf{k}_r - \mathbf{k}_{\theta}, k_{\alpha} + \frac{1}{\pi})e^{i2\theta}] \\ &+ e^{-i\phi}[\tilde{S}_p(\mathbf{k}_r + \mathbf{k}_{\theta}, k_{\alpha}) + \frac{1}{2}\tilde{S}_p(\mathbf{k}_r + \mathbf{k}_{\theta}, k_{\alpha} - \frac{1}{\pi})e^{-i2\theta} + \frac{1}{2}\tilde{S}_p(\mathbf{k}_r + \mathbf{k}_{\theta}, k_{\alpha} + \frac{1}{\pi})e^{i2\theta}] \end{aligned} \right\} \cdot OTF(\mathbf{k}_r, k_{\alpha}) \end{aligned} \quad (S6)$$

Given a specific  $\theta_i$ , there are 9 unknown variables in Eq.6:  $\tilde{S}_p(\mathbf{k}_r, k_{\alpha})$ ,  $\tilde{S}_p(\mathbf{k}_r, k_{\alpha} \pm \frac{1}{\pi})$ ,  $\tilde{S}_p(\mathbf{k}_r \pm \mathbf{k}_{\theta_i}, k_{\alpha})$ ,  $\tilde{S}_p(\mathbf{k}_r \pm \mathbf{k}_{\theta_i}, k_{\alpha} \pm \frac{1}{\pi})$ . However, we cannot solve all of these 9 variables, because they can be separate into three linear dependent groups:

$$\begin{aligned} &\tilde{S}_p(\mathbf{k}_r, k_{\alpha}), \tilde{S}_p(\mathbf{k}_r, k_{\alpha} \pm \frac{1}{\pi}) \\ &\tilde{S}_p(\mathbf{k}_r + \mathbf{k}_{\theta}, k_{\alpha}), \tilde{S}_p(\mathbf{k}_r + \mathbf{k}_{\theta}, k_{\alpha} \pm \frac{1}{\pi}) \\ &\tilde{S}_p(\mathbf{k}_r - \mathbf{k}_{\theta}, k_{\alpha}), \tilde{S}_p(\mathbf{k}_r - \mathbf{k}_{\theta}, k_{\alpha} \pm \frac{1}{\pi}) \end{aligned} \quad (S7)$$



So the coefficient matrix is singular, the linear equation cannot be resolved. We set:

$$\begin{aligned}\tilde{S}_{p0\theta_i} &= \tilde{S}_p(\mathbf{k}_r, k_\alpha) + \frac{1}{2}\tilde{S}_p(\mathbf{k}_r, k_\alpha - \frac{1}{\pi})e^{-i2\theta_i} + \frac{1}{2}\tilde{S}_p(\mathbf{k}_r, k_\alpha + \frac{1}{\pi})e^{i2\theta_i} \\ \tilde{S}_{p1\theta_i} &= \tilde{S}_p(\mathbf{k}_r - \mathbf{k}_{\theta_i}, k_\alpha) + \frac{1}{2}\tilde{S}_p(\mathbf{k}_r - \mathbf{k}_{\theta_i}, k_\alpha - \frac{1}{\pi})e^{-i2\theta_i} + \frac{1}{2}\tilde{S}_p(\mathbf{k}_r - \mathbf{k}_{\theta_i}, k_\alpha + \frac{1}{\pi})e^{i2\theta_i} \\ \tilde{S}_{p2\theta_i} &= \tilde{S}_p(\mathbf{k}_r + \mathbf{k}_{\theta_i}, k_\alpha) + \frac{1}{2}\tilde{S}_p(\mathbf{k}_r + \mathbf{k}_{\theta_i}, k_\alpha - \frac{1}{\pi})e^{-i2\theta_i} + \frac{1}{2}\tilde{S}_p(\mathbf{k}_r + \mathbf{k}_{\theta_i}, k_\alpha + \frac{1}{\pi})e^{i2\theta_i}\end{aligned}\quad (S8)$$

With the three inputs  $\phi_1, \phi_2, \phi_3$ , we can calculate these three units  $\tilde{S}_{0\theta_i}, \tilde{S}_{1\theta_i}, \tilde{S}_{2\theta_i}$  by solving the following linear equations:

$$\begin{bmatrix} \tilde{D}_{\theta_i, \phi_1}(\mathbf{k}_r, k_\alpha) \\ \tilde{D}_{\theta_i, \phi_2}(\mathbf{k}_r, k_\alpha) \\ \tilde{D}_{\theta_i, \phi_3}(\mathbf{k}_r, k_\alpha) \end{bmatrix} = M_{SIM} \cdot \begin{bmatrix} \tilde{S}_{p0\theta_i} \cdot OTF(\mathbf{k}_r, k_\alpha) \\ \tilde{S}_{p1\theta_i} \cdot OTF(\mathbf{k}_r, k_\alpha) \\ \tilde{S}_{p2\theta_i} \cdot OTF(\mathbf{k}_r, k_\alpha) \end{bmatrix}; M_{SIM} = \frac{\pi I_0}{4} \begin{bmatrix} 1 & \frac{1}{2}e^{i\phi_1} & \frac{1}{2}e^{-i\phi_1} \\ 1 & \frac{1}{2}e^{i\phi_2} & \frac{1}{2}e^{-i\phi_2} \\ 1 & \frac{1}{2}e^{i\phi_3} & \frac{1}{2}e^{-i\phi_3} \end{bmatrix} \quad (S9)$$

With three pattern directions  $\theta_1, \theta_2, \theta_3$ , we should notice that  $\tilde{S}_{p0\theta_1}, \tilde{S}_{p0\theta_2}, \tilde{S}_{p0\theta_3}$  is the linear combination of the same components  $\tilde{S}_p(\mathbf{k}_r, k_\alpha), \tilde{S}_p(\mathbf{k}_r, k_\alpha - \frac{1}{\pi}), \tilde{S}_p(\mathbf{k}_r, k_\alpha + \frac{1}{\pi})$  with different coefficients. So they can be calculated by solving following linear equations:

$$\begin{bmatrix} \tilde{S}_{p0\theta_1} \\ \tilde{S}_{p0\theta_2} \\ \tilde{S}_{p0\theta_3} \end{bmatrix} = M_{LD} \cdot \begin{bmatrix} \tilde{S}_p(\mathbf{k}_r, k_\alpha) \\ \tilde{S}_p(\mathbf{k}_r, k_\alpha - \frac{1}{\pi}) \\ \tilde{S}_p(\mathbf{k}_r, k_\alpha + \frac{1}{\pi}) \end{bmatrix}; M_{LD} = \begin{bmatrix} 1 & \frac{1}{2}e^{-i2\theta_1} & \frac{1}{2}e^{i2\theta_1} \\ 1 & \frac{1}{2}e^{-i2\theta_2} & \frac{1}{2}e^{i2\theta_2} \\ 1 & \frac{1}{2}e^{-i2\theta_3} & \frac{1}{2}e^{i2\theta_3} \end{bmatrix} \quad (S10)$$

Therefore, the one-time-frequency component  $\tilde{S}_p(\mathbf{k}_r, k_\alpha \pm \frac{1}{\pi})$  can be resolved. So the dipole orientation can be determined by applying inverse Fourier transform in the polarization dimension.

However, the 6 high-order spatial components  $\tilde{S}_p(\mathbf{k}_r \pm \mathbf{k}_{\theta_1}, k_\alpha), \tilde{S}_p(\mathbf{k}_r \pm \mathbf{k}_{\theta_2}, k_\alpha \pm \frac{1}{\pi})$  cannot be resolved. For example, under the illumination angle  $\theta_1$ , these three components  $\tilde{S}_p(\mathbf{k}_r \pm \mathbf{k}_{\theta_1}, k_\alpha), \tilde{S}_p(\mathbf{k}_r \pm \mathbf{k}_{\theta_1}, k_\alpha \pm \frac{1}{\pi})$  appear in Eq. (6). However, they are always linear dependent with each other as:

$$\begin{aligned}e^{i\phi}[\tilde{S}_p(\mathbf{k}_r - \mathbf{k}_{\theta_1}, k_\alpha) + \frac{1}{2}\tilde{S}_p(\mathbf{k}_r - \mathbf{k}_{\theta_1}, k_\alpha - \frac{1}{\pi})e^{-i2\theta_1} + \frac{1}{2}\tilde{S}_p(\mathbf{k}_r - \mathbf{k}_{\theta_1}, k_\alpha + \frac{1}{\pi})e^{i2\theta_1}] \\ e^{-i\phi}[\tilde{S}_p(\mathbf{k}_r + \mathbf{k}_{\theta_1}, k_\alpha) + \frac{1}{2}\tilde{S}_p(\mathbf{k}_r + \mathbf{k}_{\theta_1}, k_\alpha - \frac{1}{\pi})e^{-i2\theta_1} + \frac{1}{2}\tilde{S}_p(\mathbf{k}_r + \mathbf{k}_{\theta_1}, k_\alpha + \frac{1}{\pi})e^{i2\theta_1}]\end{aligned}\quad (S11)$$

It means that we can only calculate one linear combination of these components, no matter how we change the illumination phase. Moreover, this information of these components cannot be provided under  $\theta_2$  and  $\theta_3$ , so we cannot separately them theoretically.

## B. SUPPLEMENTARY NOTE 2: COMPARISON BETWEEN LD AND FA

For linear dichroism (LD) imaging system, rotational polarization modulation of excitation laser is used to excite to dipoles[2, 3]. The final excitation efficiency is a cosine-square relationship of the difference of dipole orientation  $\alpha$  and excitation polarization  $\theta$ .

$$F(\mathbf{r}, \alpha) = \eta \cos^2(\theta - \alpha) \quad (S12)$$

Therefore, the Fourier transform of  $D_\theta(\mathbf{r}, \alpha)$  can be represented as:

$$\begin{aligned}\tilde{D}_\theta(\mathbf{k}_r, k_\alpha) &= \eta[\tilde{S}_p(\mathbf{k}_r, k_\alpha) \otimes (\delta(k_\alpha) + e^{-i2\theta}\delta(k_\alpha - \frac{1}{\pi}) + e^{i2\theta}\delta(k_\alpha + \frac{1}{\pi}))] \cdot [OTF(\mathbf{k}_r, k_\alpha)], \\ &= \eta[\tilde{S}_p(\mathbf{k}_r, k_\alpha) + e^{-i2\theta}\tilde{S}_p(\mathbf{k}_r, k_\alpha - \frac{1}{\pi}) + e^{i2\theta}\tilde{S}_p(\mathbf{k}_r, k_\alpha + \frac{1}{\pi})] \cdot OTF(\mathbf{k}_r) \cdot \delta(k_\alpha).\end{aligned}\quad (S13)$$

For Fluorescence Anisotropy (FA), the emitted fluorescence polarization is separated by a polarizer with various directions or polarization beam splitter, so each detected image is corresponding to a specific detection orientation[7, 14, 15]. The  $PSF_\phi(\mathbf{r}, \alpha)$  of the detection orientation can be represented as:

$$PSF_\phi(\mathbf{r}, \alpha) = PSF(\mathbf{r}, \alpha)[1 + p\cos(2\phi - 2\alpha)], \quad (S14)$$

where  $p$  denotes the polarization degree of the signal.

In this condition, the Fourier transform of  $D_\phi(\mathbf{r}, \alpha)$  can be represented as:

$$\begin{aligned} \tilde{D}_\theta(\mathbf{k}_r, k_\alpha) &= \tilde{S}_p(\mathbf{k}_r, k_\alpha) \cdot [OTF(\mathbf{k}_r) \otimes [\delta(k_\alpha) + \frac{p}{2}e^{-j2\phi}\delta(k_\alpha - \frac{1}{\pi}) + \frac{p}{2}e^{j2\phi}\delta(k_\alpha + \frac{1}{\pi})]] \\ &= \tilde{S}_p(\mathbf{k}_r, k_\alpha) \otimes [\delta(k_\alpha) + \frac{p}{2}e^{-j2\phi}\delta(k_\alpha - \frac{1}{\pi}) + \frac{p}{2}e^{j2\phi}\delta(k_\alpha + \frac{1}{\pi})] \cdot OTF(\mathbf{k}_r)\delta(k_\alpha) \\ &= [\tilde{S}_p(\mathbf{k}_r, k_\alpha) + \frac{p}{2}e^{-i2\phi}\tilde{S}_p(\mathbf{k}_r, k_\alpha - \frac{1}{\pi}) + \frac{p}{2}e^{i2\phi}\tilde{S}_p(\mathbf{k}_r, k_\alpha + \frac{1}{\pi})] \cdot OTF(\mathbf{k}_r)\delta(k_\alpha). \end{aligned} \quad (S15)$$

In the combination of LD and FA, the Fourier space  $D_{\theta,\phi}(\mathbf{r}, \alpha)$  should be:

$$\begin{aligned} \tilde{D}_\theta(\mathbf{k}_r, k_\alpha) &= \{\tilde{S}_p(\mathbf{k}_r, k_\alpha) \otimes \eta[\delta(k_\alpha) + \frac{1}{2}e^{-j2\theta}\delta(k_\alpha - \frac{1}{\pi}) + \frac{1}{2}e^{j2\theta}\delta(k_\alpha + \frac{1}{\pi})]\} \\ &\quad \cdot [OTF(\mathbf{k}_r)\delta(k_\alpha) \otimes [\delta(k_\alpha) + \frac{p}{2}e^{-j2\phi}\delta(k_\alpha - \frac{1}{\pi}) + \frac{p}{2}e^{j2\phi}\delta(k_\alpha + \frac{1}{\pi})]] \\ &= \{[1 + \frac{p}{2}\cos^2(\theta - \phi)]S_p(\mathbf{k}_r, k_\alpha) + \frac{1}{2}(e^{j2\theta} + pe^{j2\phi})S_p(\mathbf{k}_r, k_\alpha + \frac{1}{\pi}) + \frac{1}{2}(e^{-j2\theta} + pe^{-j2\phi})S_p(\mathbf{k}_r, k_\alpha - \frac{1}{\pi}) \\ &\quad + \frac{1}{2}(e^{j2\theta} + pe^{j2\phi})S_p(\mathbf{k}_r, k_\alpha + \frac{1}{\pi}) + \frac{p}{4}e^{-j2(\theta+\phi)}S_p(\mathbf{k}_r, k_\alpha - \frac{2}{\pi}) \\ &\quad + \frac{p}{4}e^{j2(\theta+\phi)}S_p(\mathbf{k}_r, k_\alpha + \frac{2}{\pi})\} \cdot OTF(\mathbf{k}_r)\delta(k_\alpha) \end{aligned} \quad (S16)$$

As shown in (S13), (S15), (S16), LD and FA bring us the first-order frequency components, which we cannot acquire in the wild field microscopy. By combining these two methods, we can further make the second-order frequency components detected.

### C. SUPPLEMENTARY NOTE 3: NONLINEAR POLARIZED EXCITATION

Linearly polarized excitation could generate sinusoidal or linear structured illumination pattern on the polarization dimension. Two Photon Excitation (TPE) and Excitation Polarization Angle Narrowing (ExPAN) could generate nonlinear structured illumination pattern, which contains more frequency components and brings higher resolution on polarization dimension.

TPE could be described by an absorptivity tensor of the fluorescent dipoles, whose effects of dipole orientation are generally complex[18]. Two-photon excitation efficiency is proportional to the fourth power of the angle difference for some rod-like molecules[19]. The structured illumination  $F_{TPE}(\alpha) = \cos^4(\alpha - \theta)$  contains both zero-frequency, first-order-frequency, and second-order-frequency components, which would achieve the same polarization resolution as LD + FA methods (**Figure S2 a**).

ExPAN is another type of nonlinear polarized excitation utilizing stimulated excitation depletion[3]. When the excitation beam and depletion beam have perpendicular polarizations, the fluorescence output could be described by

$$F_{ExPAN}(\alpha) = \frac{k_{0,exc}\cos(\alpha - \theta)}{k_{fl} + k_{0,exc}\cos^2(\alpha - \theta) + k_{0,SE}\cos^2(\alpha - \theta + \frac{\pi}{2})}, \quad (S17)$$

where  $k_{0,exc}$  denotes the rate constant for excitation,  $k_{0,SE}$  denotes the fluorescence decay state,  $k_{fl}$  denotes the rate constant for stimulated emission. The modulation curve varies with the extinction rate, or  $k_{0,SE}/k_{0,exc}$ . In **Figure S2 b**,  $k_{0,SE} = 10k_{0,exc}$ ,  $k_{fl} = 0.1k_{0,exc}$  and in **Figure S2 c**,  $k_{0,SE} = 20k_{0,exc}$ ,  $k_{fl} = 0.1k_{0,exc}$ . The higher extinction rate, the more frequency components would appear, resulting higher polarization resolution.

## D. SUPPLEMENTARY FIGURES

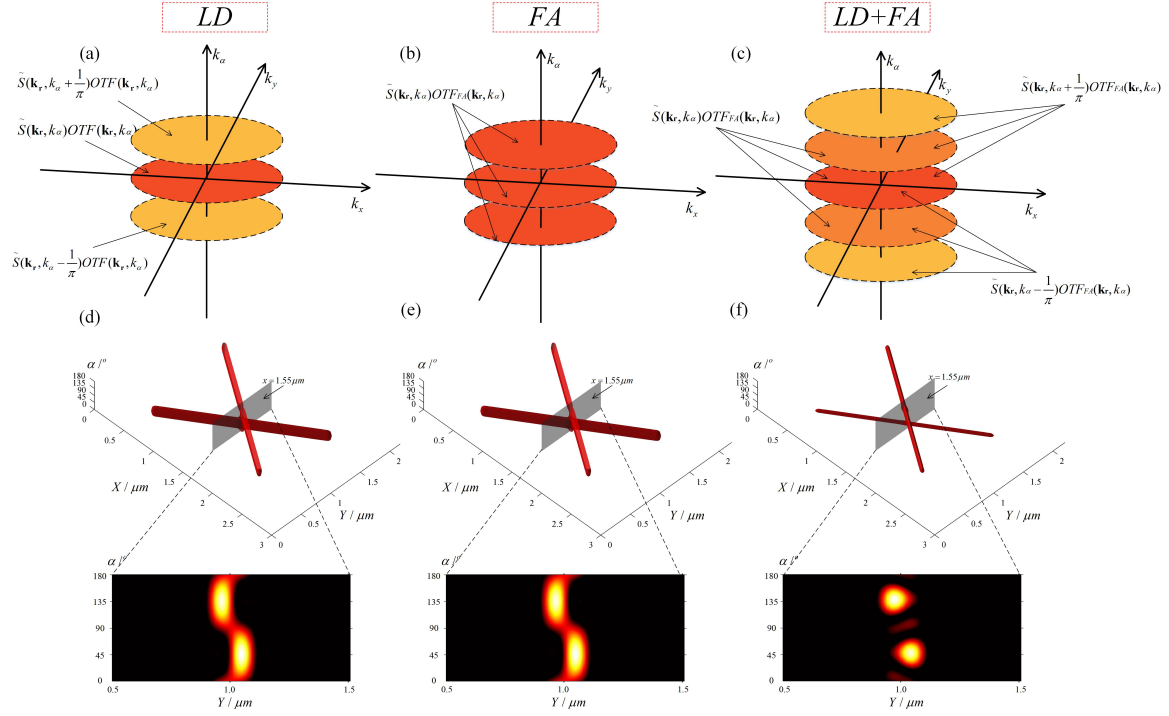


**Figure S1: Comparison among LD, FA and LD+FA by structured illumination theory.** (a) The three frequency components are shown in reciprocal space of LD; (b) The system OTF of FA has both zero-frequency component and one-time-frequency components in polarization dimension; (c) With LD further expanding the detected FA frequency components, two-time-frequency components could be obtained as well; (d-f) The simulation results of two intersecting lines with the dipole orientations perpendicular to their direction are demonstrated, where the lower subfigures are sectional view of the corresponding upper ones at the plane  $x = 1.55\mu\text{m}$ . Since LD and FA contains one-time-frequency components, the detected intensity profile on polarization axis is sinusoidal. The LD+FA method contains higher frequency components so that the detected two dipole orientations are separated more thoroughly.

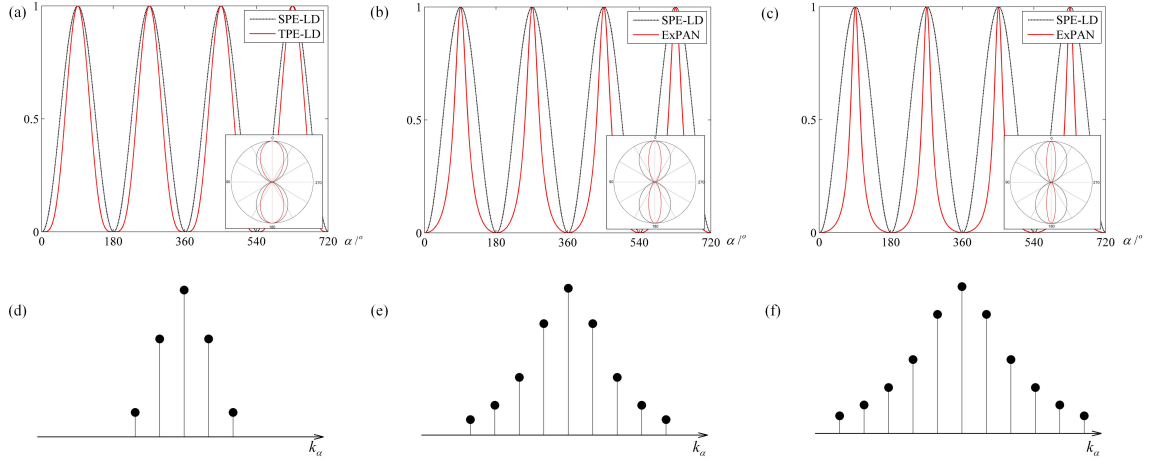


Figure S2: **Comparison between TPE-LD and ExPAN.** (a) Polarization excitation of TPE on fluorescent dipoles with different orientations. (b, c) Polarization excitation of ExPAN on fluorescent dipoles with different orientations. The different extinction rates in (b, c) are indicated in **Supplementary Note 3**. (d-f) The corresponding frequency components of (a-c) in reciprocal space.

## REFERENCES

- [1] Bradley S DeMay, Naoki Noda, Amy S Gladfelter, and Rudolf Oldenbourg. Rapid and quantitative imaging of excitation polarized fluorescence reveals ordered septin dynamics in live yeast. *Biophysical journal*, 101(4):985–994, 2011.
- [2] Karl Zhanghao, Long Chen, Xu San Yang, Miao Yan Wang, Zhen Li Jing, Hong Bin Han, Michael Q Zhang, Dayong Jin, Jun Tao Gao, and Peng Xi. Super-resolution dipole orientation mapping via polarization demodulation. *Light Science & Applications*, 5(10):e16166, 2016.
- [3] Peter J. Walla, Nour Hafi, Matthias Grunwald, Laura Van Den Heuvel, Aspelmeier Timo, Marta Zagrebelsky, Martin Korte, and Axel Munk. Fluorescence nanoscopy by polarization modulation and polarization angle narrowing. *Nature Methods*, 11(9):579–584, 2016.
- [4] Alicja Gasecka, Tsai-Jung Han, Cyril Favard, Bong Rae Cho, and Sophie Brasselet. Quantitative imaging of molecular order in lipid membranes using two-photon fluorescence polarimetry. *Biophysical journal*, 97(10):2854–2862, 2009.
- [5] Josef Lazar, Alexey Bondar, Stepan Timr, and Stuart J Firestein. Two-photon polarization microscopy reveals protein structure and function. *Nature methods*, 8(8):684–690, 2011.
- [6] Alina M Vrabioiu and Timothy J Mitchison. Structural insights into yeast septin organization from polarized fluorescence microscopy. *Nature*, 443(7110):466–469, 2006.
- [7] Joseph N Forkey, Margot E Quinlan, M Alexander Shaw, John ET Corrie, and Yale E Goldman. Three-dimensional structural dynamics of myosin v by single-molecule fluorescence polarization. *Nature*, 422(6930):399–404, 2003.
- [8] Takayuki Nishizaka, Kazuhiro Oiwa, Hiroyuki Noji, Shigeki Kimura, Eiro Muneyuki, Masasuke Yoshida, and Kazuhiko Kinoshita. Chemomechanical coupling in f1-atpase revealed by simultaneous observation of nucleotide kinetics and rotation. *Nature structural & molecular biology*, 11(2):142–148, 2004.
- [9] Martin Kampmann, Claire E Atkinson, Alexa L Mattheyses, and Sanford M Simon. Mapping the orientation of nuclear pore proteins in living cells with polarized fluorescence microscopy. *Nature structural & molecular biology*, 18(6):643–649, 2011.
- [10] C. A. Valades Cruz, H. A. Shaban, A Kress, N Bertaux, S Monneret, M Mavrikakis, J Savatier, and S Brasselet. Quantitative nanoscale imaging of orientational order in biological filaments by polarized superresolution microscopy. *Proceedings of the National Academy of Sciences*, 113(7):E820, 2016.
- [11] Adam S. Backer, Maurice Y. Lee, and W. E. Moerner. Enhanced dna imaging using super-resolution microscopy and simultaneous single-molecule orientation measurements. *Optica*, 3(6):659–666, Jun 2016.
- [12] Erdal Toprak, Joerg Enderlein, Sheyum Syed, Sean A. McKinney, Rolfe G. Petschek, Taekjip Ha, Yale E. Goldman, and Paul R. Selvin. Defocused orientation and position imaging (dopi) of myosin v. *Proceedings of the National Academy of Sciences*, 103(17):6495–9, 2006.
- [13] Mikael P. Backlund and W. E. Moerner. Simultaneous, accurate measurement of the 3d position and orientation of single molecules. *Proceedings of the National Academy of Sciences of the United States of America*, 109(47):19087–92, 2012.
- [14] Shalin B Mehta, Molly McQuilken, Patrick J La Riviere, Patricia Occhipinti, Amitabh Verma, Rudolf Oldenbourg, Amy S Gladfelter, and Tomomi Tani. Dissection of molecular assembly dynamics by tracking orientation and position of single molecules in live cells. *Proceedings of the National Academy of Sciences*, 113(42):E6352–E6361, 2016.
- [15] Yujie Sun, Osamu Sato, Felix Ruhnnow, Mark E Arsenault, Mitsuo Ikebe, and Yale E Goldman. Single-molecule stepping and structural dynamics of myosin x. *Nature structural & molecular biology*, 17(4):485–491, 2010.

- [16] Dong Li, Lin Shao, Bi-Chang Chen, Xi Zhang, Mingshu Zhang, Brian Moses, Daniel E Milkie, Jordan R Beach, John A Hammer, Mithun Pasham, et al. Extended-resolution structured illumination imaging of endocytic and cytoskeletal dynamics. *Science*, 349(6251):aab3500, 2015.
- [17] Tyler C Schlichenmeyer, Mei Wang, Katherine N Elfer, and J Quincy Brown. Video-rate structured illumination microscopy for high-throughput imaging of large tissue areas. *Biomedical optics express*, 5(2):366–377, 2014.
- [18] Patrik R. Callis. *The Theory of Two-Photon-Induced Fluorescence Anisotropy*. Springer US, 2002.
- [19] S. Y. Chen and Van Der Meer Bw. Theory of two-photon induced fluorescence anisotropy decay in membranes. *Biophysical Journal*, 64(5):1567–75, 1993.